



# Solution of the Inverse Jet in a Crossflow Problem by a Predictor-Corrector Technique

Joseph R VanderVeer, Yogesh Jaluria\*

*Department of Mechanical and Aerospace Engineering: Rutgers University, 98 Brett Rd,  
Piscataway NJ, 08854*

---

## Abstract

*Keywords:* Inverse Problems, Computational Heat Transfer, Convection

---

## 1. Introduction

Thermal-fluid systems often create situations where the engineering problem is an inverse heat transfer problem. These problems often have limited physical access, very limited to no boundary condition knowledge, and/or limited domain knowledge.

For example, the temperature distribution of an optical fiber drawing furnace is difficult to measure directly due to shape, inaccessibility, and high temperatures. The center of the furnace is easily accessible and this directly leads to an inverse heat transfer problem. Issa et al. [1] [1] developed a regularization technique utilizing the centerline temperature from which the wall temperature may be obtained.

Another example, is the inverse plume in a crossflow problem. The problem entails solving for the plume boundary conditions utilizing limited domain knowledge. A novel predictor-corrector method was developed by VanderVeer and Jaluria [2] [2] to solve such a problem. The method requires

---

\*Corresponding Author

*Email address:* jaluria@soemail.rutgers.edu (Yogesh Jaluria)



due to material limitations of the wind tunnel. The X-direction is directed downstream of the wind tunnel with the zero at the center of the jet. The Y-direction is in the direction of the jet and is zero at the surface of the wind tunnel. Due to the large aspect ratio of the wind tunnel the flow is assumed to be two-dimensional.

The free stream velocity is determined by a Pitot-Static tube attached to a NIST traceable differential pressure sensor from Omega(PX655-0.1DI). The pressure sensor has a full scale reading of 0.1 inches of water and is accurate to 0.05% of full scale. This results in a maximum of 3% error of the calculated velocity.

The jet velocity is determined utilizing a rotameter and verified using a Pitot-Static tube attached to the same previously described pressure sensor. This results in the same amount of error of 3% for the jet velocity.

The temperature of domain is measured using a K-type thermocouple mounted to an X-Y traversing stage. Sampled data over the course of several days indicate repeatability of the experiment to within 2%.

### 3. Numerical Simulations

The simulations were all performed using Ansys Fluent[3]. The Navier-Stokes equations were solved using a three-dimensional, steady state, realizable  $k - \epsilon$  model with enhanced wall effects. Conjugate heat transfer is modelled. The free stream Reynolds number is of order  $6 \times 10^3$ , while the jet Reynolds number is between  $10^3$  and  $10^4$ . The Rayleigh number is of order  $10^7$ .

The governing equations are expressed below:

$$u_i = \overline{u_i} + u_i' \quad (1)$$

$$\frac{\partial \rho}{\partial t} + \frac{\partial}{\partial x_i} (\rho u_i) = 0 \quad (2)$$

$$\begin{aligned} \frac{\partial}{\partial t} (\rho u_i) + \frac{\partial}{\partial x_j} (\rho u_i u_j) = \\ \frac{\partial P}{\partial x_i} + \frac{\partial}{\partial x_j} \left[ \mu \left( 2S_{ij} - \frac{2}{3} \delta_{ij} \frac{\partial u_k}{\partial x_k} \right) - \rho \overline{u_i' u_j'} \right] \end{aligned} \quad (3)$$

$$\begin{aligned} \frac{\partial}{\partial t} (\rho E) + \frac{\partial}{\partial x_i} [u_i (\rho E + P)] = \\ \frac{\partial}{\partial x_i} \left[ \left( \lambda + \frac{C_p \mu_t}{P_{rt}} \right) \frac{\partial T}{\partial x_i} \right] \end{aligned} \quad (4)$$

$$\begin{aligned} \frac{\partial}{\partial t} (\rho k) + \frac{\partial}{\partial x_j} (\rho k u_j) = \\ \frac{\partial}{\partial x_j} \left[ \left( \mu + \frac{\mu_t}{\sigma_k} \right) \frac{\partial k}{\partial x_j} \right] + \frac{\partial u_j}{\partial x_i} \left( -\rho \overline{u'_i u'_j} \right) \\ - g_i \frac{\mu_t}{\rho P_{rt}} \frac{\partial \rho}{\partial x_i} + \rho \epsilon \end{aligned} \quad (5)$$

$$\begin{aligned} \frac{\partial}{\partial t} (\rho \epsilon) + \frac{\partial}{\partial x_j} (\rho \epsilon u_j) = \\ \frac{\partial}{\partial x_j} \left[ \left( \mu + \frac{\mu_t}{\sigma_\epsilon} \right) \frac{\partial \epsilon}{\partial x_j} \right] + \rho C_1 S \epsilon - \rho C_2 \frac{\epsilon^2}{k + \sqrt{\nu \epsilon}} \\ - C_{1\epsilon} \frac{\epsilon}{k} C_{3\epsilon} g_i \frac{\mu_t}{\rho P_{rt}} \frac{\partial \rho}{\partial x_i} \end{aligned} \quad (6)$$

$$-\rho \overline{u'_i u'_j} = 2\mu_t S_{ij} - \frac{2}{3} \delta_{ij} \left( \rho k + \mu_t \frac{\partial u_k}{\partial x_k} \right) \quad (7)$$

The constants for the turbulence model are [4, 5] :

$$C_{1\epsilon} = 1.44, C_2 = 1.9, \sigma_k = 1.0, \sigma_\epsilon = 1.2, P_{rt} = 0.85 \quad (8)$$

$$C_1 = \max \left[ 0.43, \frac{Sk/\epsilon}{Sk/\epsilon + 5} \right], S = \sqrt{2S_{ij}S_{ji}}, C_{3\epsilon} = \tanh \left( \frac{u_g}{u_p} \right) \quad (9)$$

$$\mu_t = \frac{\rho C_\mu k^2}{\epsilon} \quad (10a)$$

$$C_\mu = \frac{1}{A_0 + \frac{A_1 k U^*}{\epsilon}} \quad (10b)$$

$$U^* \equiv \sqrt{S_{ij}S_{ji} + \Omega_{ij}\Omega_{ji}} \quad (10c)$$

$$A_0 = 4.04 \quad (10d)$$

$$A_1 = \sqrt{6} \cos \left[ \frac{1}{3} \cos^{-1} \left( \sqrt{6} \frac{S_{ij}S_{jk}S_{ki}}{(S_{ij}S_{ji})^{\frac{3}{2}}} \right) \right] \quad (10e)$$

$$S_{ij} = \frac{1}{2} \left( \frac{\partial u_i}{\partial x_j} + \frac{\partial u_j}{\partial x_i} \right) \quad (10f)$$

$$\Omega_{ij} = \frac{1}{2} \left( \frac{\partial u_i}{\partial x_j} - \frac{\partial u_j}{\partial x_i} \right) \quad (10g)$$

Where the  $u_g$  and  $u_p$  are the velocity component parallel and perpendicular to gravity respectively.

The inflow boundary conditions are:

$$u = U_\infty, v = 0, T = T_\infty, P = P_\infty, l = 4mm, I = 5\% \quad (11a)$$

$$k = \frac{3}{2} (U_\infty I)^2 \quad (11b)$$

$$\epsilon = C_\mu^{3/4} \frac{k^{3/2}}{l} \quad (11c)$$

The jet inflow boundary conditions are:

$$u = 0, v = U_S, T = T_S, P = P_\infty, l = 4mm, I = 5\% \quad (12a)$$

$$k = \frac{3}{2} (U_\infty I)^2 \quad (12b)$$

$$\epsilon = C_\mu^{3/4} \frac{k^{3/2}}{l} \quad (12c)$$

The upper boundary was taken to be symmetric to reduce the possibility of errors by the experimentally accurate no-slip condition. The upper boundary is very far from the jet and therefore should have negligible effect on the numerical result. The bottom of the wind tunnel is made up of 12 mm thick

Parameter	Value
$U_\infty (m/s)$	$2.0 \pm 0.02$
$U_S (m/s)$	$2.0 \pm 0.2$
$T_\infty (K)$	$305 \pm 0.5$
$P_\infty (kPa)$	$101.3 \pm 0.01$
$T_S (K)$	$350 \pm 2.0$

Table 1: Validation test conditions

acrylic, while the test section is 25.4 mm thick acrylic. The external boundary conditions are iso-thermal with a temperature of  $T_\infty$ . The test section external temperature is iso-thermal of  $\frac{1}{2}(T_S + T_\infty)$ . The outflow boundary is a simple pressure outflow of  $P_\infty$ .

### 3.1. Simulation Validation

A simulation validation study was performed to verify the results of the simulations. Typical verification was performed including flow model, grid independence, and comparison with experimental results. The conditions of the simulation validation are shown in table 1.

The results from Spalart-Allmaras,  $k - \epsilon$ , and  $k - \omega$  were compared and the three models have a similar trend. SA tends to be a bit off, but this is expected due to issues with this type of problem[5]. All of the values were normalized utilizing the following equations, where  $D$  is the width of the jet. Figure 2 shows a comparison of the flow models at  $X = 4.75$ .

$$\phi = \frac{T - T_\infty}{T_S - T_\infty} \quad (13a)$$

$$X = \frac{x}{D} \quad (13b)$$

$$Y = \frac{y}{D} \quad (13c)$$

$$V = \frac{U}{U_\infty} \quad (13d)$$

$$V_S = \frac{U_S}{U_\infty} \quad (13e)$$

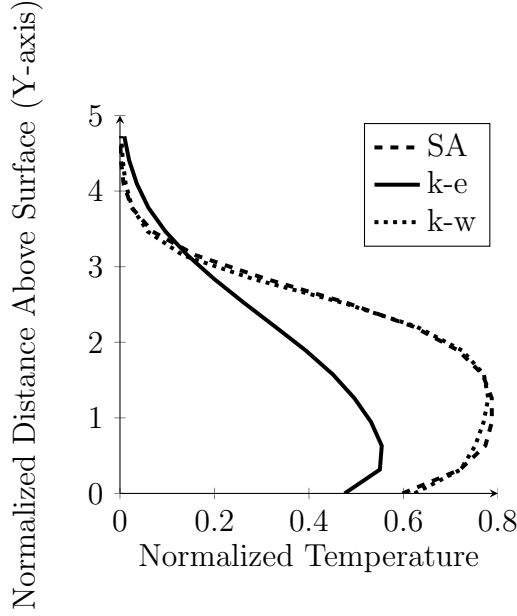


Figure 2: Validation of the simulation: local temperature using three flow models at  $X = 4.75$

Grid independence is demonstrated by testing the temperature at a few locations with various grid sizes and geometries, as shown in table 2. Very little variation in simulated temperature over such a wide variety of cell counts shows that the result is most likely grid independent. The grid employed is an unstructured hexagonal mesh with refinement located near the jet and down stream of the jet.

The final validation is comparing the simulation against the experiment. This is done in figure 3. The simulation matches the experiment closely, with the exception of very close to the wall. This is to be expected as the flow models used, even with enhanced wall effects, have difficulty perfectly modelling the near wall conditions.

#### 4. Inverse Solution Methodology

The basis for the solution strategy was described in a paper by VanderVeer and Jaluria [2], which was originally intended to solve the inverse plume in a crosswind. The original methodology solved for the 2-D location and source strength of a plume in a crossflow. The jet in a crossflow must handle one

Location (x,y) (mm)	0,1	10,5	15,5	30,10
Cell Count				
57660	337.7	323.3	321.6	310.1
83888	337.7	323.3	321.6	310.1
166352	337.7	323.2	321.5	310.1
366168	337.7	323.2	321.5	310.1

Table 2: Grid Independence Study, local static temperature (K)

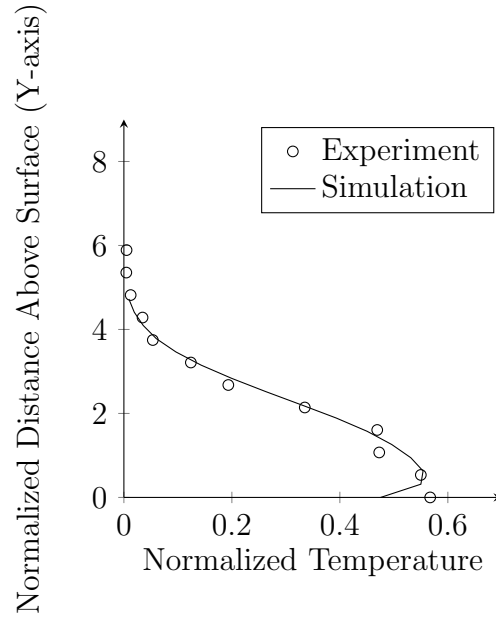


Figure 3: Validation of the simulation: local temperature - experiment versus simulation at  $X = 4.75$



$U_S$ (m/s)	1	1	2	2	4	4
$T_S$ (K)	375	425	375	425	375	425
Location (x,y)						
10 mm, 1 mm	A	B	C	D	E	F
10 mm, 3 mm	G	H	I	J	K	L
20 mm, 1 mm	M	N	O	P	Q	R
20 mm, 3 mm	S	T	U	V	W	X

Table 3: Several sampled case parameters

additional parameter, the jet velocity. Due to this extra parameter a modified version of the original solution strategy will be presented here.

[?] used a quadratic response surface model to determine the jet temperature and jet velocity. This method is not easily adapted to include unknown source location.

## 5. Results and discussions

Parameter	Value
$U_\infty$ (m/s)	2
$T_\infty$ (K)	293
$P_\infty$ (kPa)	101.3

Table 4: Simulation test conditions

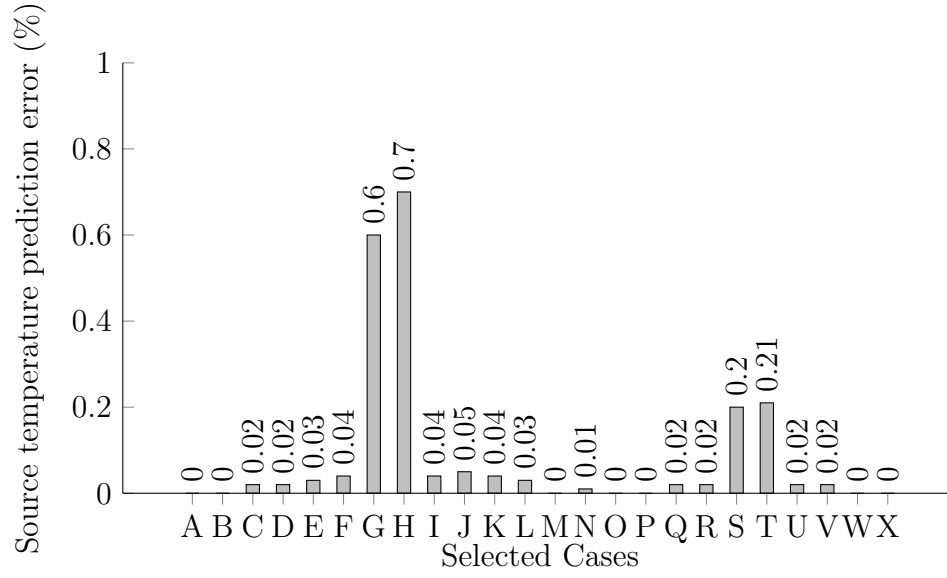


Figure 4: Error in the prediction of  $T_S$  from several sampled cases within the jet with  $r_S$  and  $U_S$  known

Axial Loc. ( $mm$ )	Elev. Loc. ( $mm$ )	Jet Temp. ( $K$ )	Jet Vel. ( $m/s$ )	Search Shape Error (%)
20.0	3.0	425	2.0	0.00
10.0	3.7	375	2.5	0.60
12.0	5.1	375	3.0	0.34
14.8	2.7	400	2.0	0.30
16.3	4.5	400	2.5	0.26
19.5	5.9	400	3.0	0.29
21.8	5.0	425	2.5	0.24
25.6	6.5	425	3.0	0.34
25.2	3.2	450	2.0	0.13
26.8	5.4	450	2.5	0.25

Table 5: Example alternative solutions

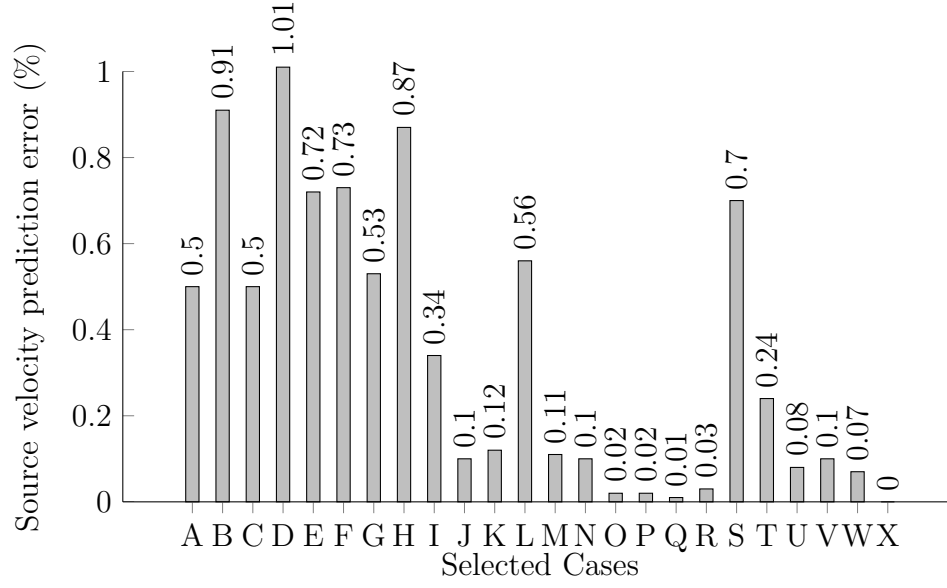


Figure 5: Error in the prediction of  $U_S$  from several sampled cases within the jet with  $r_S$  and  $T_S$  known

Parameter	Value
$T_{\infty} (K)$	$297.6 \pm 8.0$
$P_{\infty} (kPa)$	$100.6 \pm 0.6$
$U_{\infty} (m/s)$	$2.0 \pm 0.02$

Table 6: Experimental test conditions

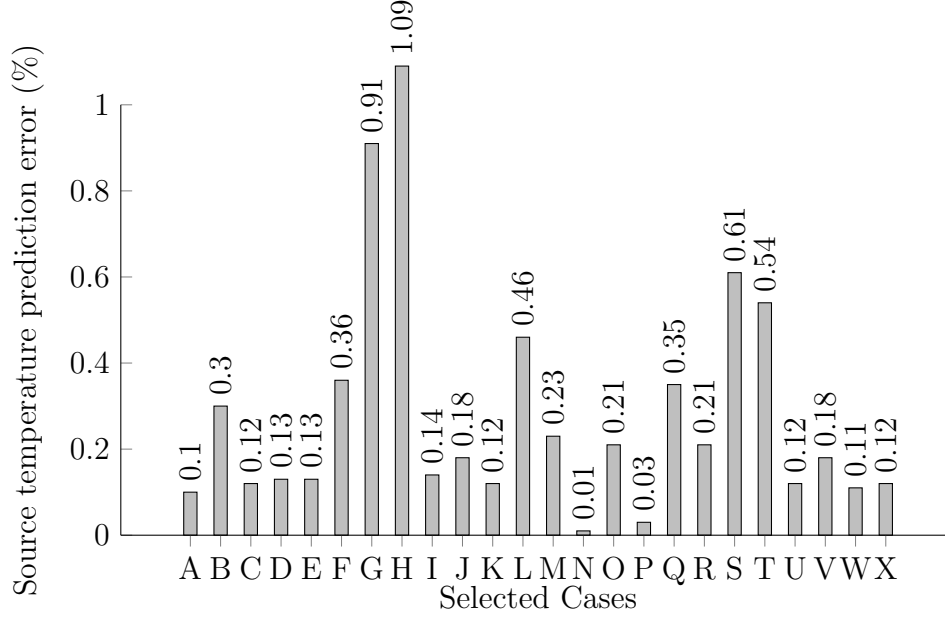


Figure 6: Error in the prediction of  $T_S$  from several sampled cases within the jet with  $r_S$  known

$U_S$ (m/s)		1.0	1.0	4.0	4.0
$T_S$ (K)		375	425	375	425
<hr/>					
Location (x,y)					
10 mm, 0 mm	X	10.9%	11.7%	11.1%	13.8%
	U	21.8%	18.6%	10.4%	11.9%
	T	8.70%	9.87%	10.7%	12.9%
20 mm, 0 mm	X	8.65%	7.65%	5.40%	9.81%
	U	18.7%	19.8%	11.5%	12.1%
	T	8.81%	10.7%	9.65%	10.2%
30 mm, 0 mm	X	10.6%	10.4%	18.7%	9.78%
	U	15.8%	17.9%	12.3%	13.7%
	T	9.61%	8.64%	13.7%	10.1%

Table 7: Error in predicting source axial location ( $x_S$ ), source strength( $U_S$  and  $T_S$ ) from a few sample cases within the jet, search shape with 9pts, utilizing experimental data

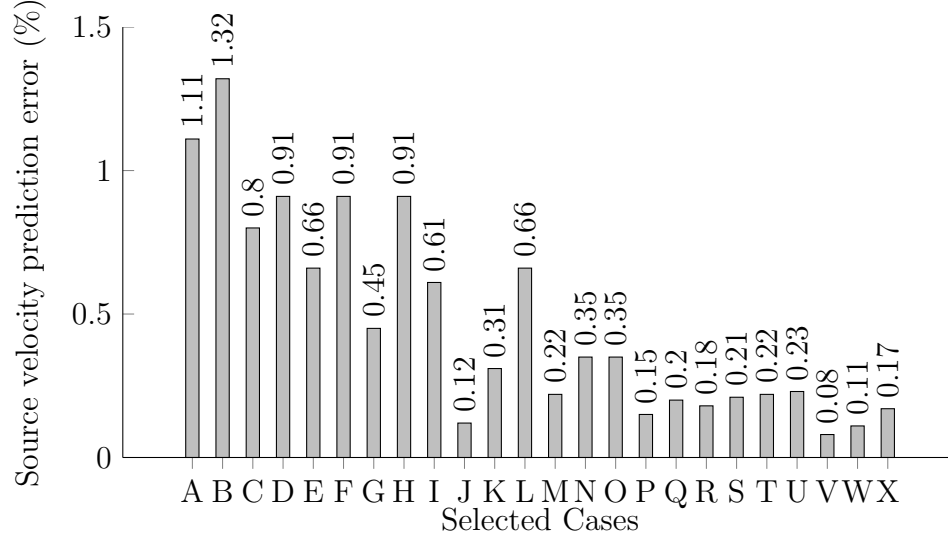


Figure 7: Error in the prediction of  $U_S$  from several sampled cases within the jet with  $r_S$  known

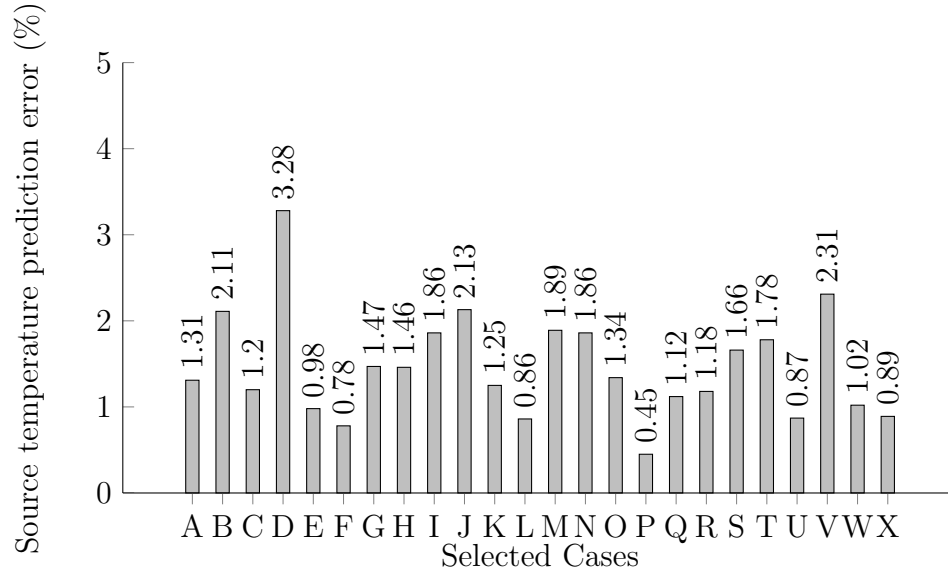


Figure 8: Error in the prediction of  $T_S$  from several sampled cases within the jet with source elevation known

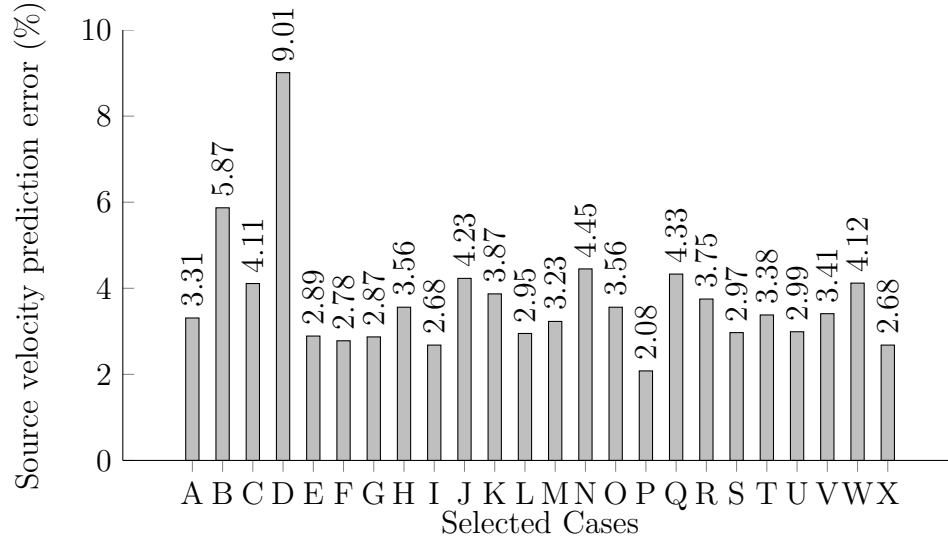


Figure 9: Error in the prediction of  $U_S$  from several sampled cases within the jet with source elevation known

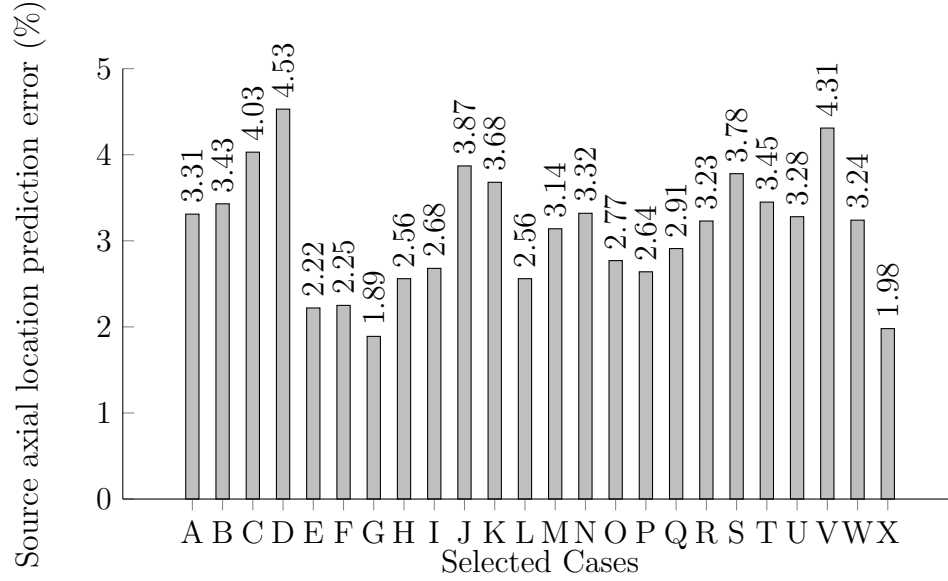


Figure 10: Error in the prediction of  $x_S$  from several sampled cases within the jet with source elevation known

- 5.1. *Source Location and Velocity Known*
- 5.2. *Source Location and Temperature Known*
- 5.3. *Source Location Known*
- 5.4. *Source Elevation Known*
- 5.5. *Source Location and Strength Unknown*
- 5.6. *Experimental Results*

## 6. Conclusions

## References

- [1] J. Issa, Z. Yin, C. E. Polymeropoulos, Y. Jaluria, Temperature distribution in an optical fiber draw tower furnace, *Journal of Materials Processing and Manufacturing Science* vol 4 (1996) 221–232.
- [2] J. VanderVeer, Y. Jaluria, Solution of an inverse convection problem by a predictor-corrector approach, *International Journal of Heat and Mass Transfer* vol65 (2013) 123–130.
- [ ] J. VanderVeer, Y. Jaluria, Optimization of an inverse convection solutions strategy, *International Journal of Heat and Mass Transfer* 73 (2014) 664–670.
- [3] Ansys, Fluent (version 13), 2010.
- [4] T. hsing Shih, W. Liou, A. Shabbir, Z. Yang, J. Zhu, A new  $k - \epsilon$  eddy viscosity model for high reynolds number turbulent flows, *Computer Fluids* vol 24 (1995) 227–238.
- [5] Ansys, Fluent Technical Documents v14.0, Technical Report, Ansys, 2011.
- [ ] D. Knight, Q. Ma, T. Rossmann, Y. Jaluria, Evaluation of fluid-thermal systems by dynamic data driven application systems - part ii, in: *International Conference on Modeling and Optimization of Structures, Processes and Systems*, Springer-Verlag, University of Kwazulu-Natal, South Africa, 2007.